




# Large heat-capacity jump in cooling-heating of fragile glass from kinetic Monte Carlo simulations based on a two-state picture

Chun-Shing Lee <sup>1</sup>, Hai-Yao Deng <sup>2</sup>, Cho-Tung Yip,<sup>3</sup> and Chi-Hang Lam <sup>1,\*</sup>

<sup>1</sup>*Department of Applied Physics, Hong Kong Polytechnic University, Hong Kong, China*

<sup>2</sup>*School of Physics and Astronomy, Cardiff University, Cardiff CF24 3AA, Wales, UK*

<sup>3</sup>*Department of Physics, Shenzhen Graduate School, Harbin Institute of Technology, Shenzhen 518055, China*



(Received 18 May 2021; accepted 3 August 2021; published 25 August 2021)

The specific-heat capacity  $c_v$  of glass formers undergoes a hysteresis when subjected to a cooling-heating cycle, with a larger  $c_v$  and a more pronounced hysteresis for fragile glasses than for strong ones. Here we show that these experimental features, including the unusually large magnitude of  $c_v$  of fragile glasses, are well reproduced by kinetic Monte Carlo and equilibrium study of a distinguishable particle lattice model incorporating a two-state picture of particle interactions. The large  $c_v$  in fragile glasses is caused by a dramatic transfer of probabilistic weight from high-energy particle interactions to low-energy ones as temperature decreases.

DOI: [10.1103/PhysRevE.104.024131](https://doi.org/10.1103/PhysRevE.104.024131)

## I. INTRODUCTION

Many fascinating aspects of glass transition rest with their nonequilibrium nature as seen in the history dependence of the thermodynamic and kinetic behaviors of glass formers [1,2]. In this work, we study long known puzzles related to their specific-heat capacity  $c_v$ . When subjected to a cooling-heating cycle,  $c_v$  exhibits a rather abrupt jump between corresponding values for liquid and glass close to the glass transition temperature. Glasses can be broadly classified as fragile or strong, depending on the degree of deviation from Arrhenius behaviors. Perplexingly, the jump magnitude of  $c_v$  is surprisingly large for fragile glasses, such as typical organic and polymeric glasses, and can reach a few  $k_B$  per particle, where  $k_B$  is the Boltzmann constant and a particle can represent an atom, a molecule or a rigid group of atoms, for example, for metallic glasses [3], small-molecule organic glasses, and polymeric glasses [4], respectively. It is in contrast much smaller for strong glasses such as silicates [5]. In addition, one also observes hysteresis in  $c_v$  during heating and cooling [6–12], which is much more pronounced for fragile glasses [9,12]. Phenomenological descriptions of  $c_v$  and the hysteresis have been advanced by mean-field theories based on a fictive temperature [7,13]. A fundamental reason for the dependence on fragility remains elusive. The phenomena have so far lacked atomistic simulations. One challenge, for example, is that molecular dynamics (MD) simulations [14,15] can hardly cope with sufficiently low cooling and heating rates entailing long computational time. This is despite the tremendous speed up in equilibrium simulations made possible by recently advanced swap Monte Carlo algorithms [16], which nevertheless cannot be applied to nonequilibrium MD simulations under heating and cooling conditions.

Lattice models play pivotal roles in many branches of statistical physics as they highlight the essential physics and

achieve superior computational speed via omitting irrelevant details [17,18]. To study glasses, most lattice models, including kinetically constrained models (KCM) [19,20] and lattice glass models [21], focus primarily on the kinetics and are energetically trivial with a vanishing  $c_v$  [22,23]. Generalizations to energetic variants, however, give  $c_v$  way smaller than typical values observed for fragile glasses [24–26]. It was argued that defect models, as most of these models are, cannot intrinsically capture the thermodynamics of glass [27]. For example,  $c_v$  in the two-spin facilitation model, an important KCM, is proportional to the defect density and thus becomes very small at low temperatures [24]. Only after coupling a lattice model to a fictive temperature field in an ad hoc fashion,  $c_v$  can be freely fine-tuned and match realistic values [8]. Nevertheless, it appears that lattice models by themselves, without any coupled field, are intrinsically incapable of capturing the correct magnitude of  $c_v$ . This severely limits their usefulness in studying glass thermodynamics and, strangely, is at odds with the stronger roles of lattice models in many other branches of statistical physics [17,18]. In addition, conventional lattice models in general cover only a limited range of fragility. This imposes another major difficulty in investigating the fragility dependence of glass thermodynamics.

Here we show that a recently proposed distinguishable particle lattice model (DPLM) [28] naturally captures the major experimentally observed thermodynamic features of glass, including the large value of  $c_v$  and the hysteresis. The close correlation of these features with fragility is also clearly demonstrated. This is made possible by the capability of the DPLM to simulate both strong and fragile glasses, with respective characteristic properties already demonstrated to be consistent with experimental trends [29].

## II. MODEL

The DPLM assumes  $N$  hard-core particles, each representing a rigid molecular group of atoms. They live on a square lattice of size  $L^2 > N$ , with the lattice constant set to unity.

\*C.H.Lam@polyu.edu.hk

Each particle is of its own species indexed by  $s = 1, 2, \dots, N$  and hence distinguishable. The total energy of the system is given by

$$E = \sum_{\langle i,j \rangle} V_{s_i s_j}, \quad (1)$$

where the sum runs over all pairs of nearest-neighboring sites occupied by particles. The energy per particle is  $\varepsilon = E/N$ .

Thermodynamic properties of glasses of various fragilities have been successfully accounted for using a simple two-state model, also called the bond-excitation model, of Moynihan and Angell, which assumes particle interactions taking independently one of two possible strengths [30]. To incorporate the two-state picture into the fully atomistic and dynamical DPLM, we sample the particle interaction energies  $V_{kl}$  for all particle pairs  $k$  and  $l$  from a *bicomponent* form of the interaction distribution  $g(V)$  before a simulation commences. It consists of a uniform low-energy part and a sharp high-energy component represented by a delta function,

$$g(V) = \frac{G_0}{\Delta V} + (1 - G_0)\delta(V - V_1), \quad (2)$$

where  $V \in [V_0, V_1]$  with  $V_0 = -V_1 = -0.5$  and  $\Delta V = V_1 - V_0 = 1$  serves as the unit of energy. In addition,  $\delta$  denotes the Dirac function which may be replaced by some narrowly peaked distributions (e.g., a Gaussian) without affecting the results, and  $G_0 \in [0, 1]$  is an energetic parameter that controls the thermodynamic properties of the system.

Unlike many other lattice models, the DPLM is intrinsically a particle model, a property essential for the direct study of the thermodynamics as particles, rather than defects, should dominate the system energy. A defect in the DPLM is instead represented implicitly by the absence of a particle, i.e., a void. We envision a void as a unit of free volume, which was long known to be important in glassy dynamics [31]. Its relevance has been disputed more than a decade ago [32]. However, sophisticated machine learning approaches have recently correlated mobility with local particle density [33,34]. We have also directly identified quasi-voids, each consisting of localized and fragmented free volumes, in colloidal experiments at very high packing fractions [35]. Using the Metropolis algorithm, a particle can move to an adjacent void at the following rate [29]

$$w = \begin{cases} w_0 \exp(-\Delta E/k_B T), & \text{for } \Delta E > 0 \\ w_0, & \text{for } \Delta E \leq 0 \end{cases} \quad (3)$$

where  $\Delta E$  is the change in the system energy due to the hop,  $T$  is the bath temperature,  $w_0 = 10^6$  is the attempt frequency, and  $k_B = 1$  is the Boltzmann constant.

It has been shown that a smaller (but finite)  $G_0$  leads to fragile glasses while a larger  $G_0$  to strong glasses [29]. By tuning  $G_0$ , a wide range of fragility can be realized. To understand it intuitively, first note that particles freely move at high  $T$  regardless of the value of  $G_0$ . At low  $T$ , particle pairings with low-energy interactions are favored but they are rare at small  $G_0$ . The number of accessible configurations with energetically favorable interactions then drop dramatically as  $T$  decreases. This results in a drastic slowdown in the dynamics, and those systems are thus fragile [29].

### III. CALORIMETRIC ANALYSIS

Throughout this work, we consider a constant void density  $\phi_v = 1 - N/L^2 = 0.01$  for simplicity. A more realistic temperature dependent  $\phi_v$  have been studied in Ref. [29] which in general gives similar qualitative features. We focus mainly on  $G_0 = 0.01$  and 1. As indicated by an Angell plot and by extrapolating simulation results to realistic timescales, they are found to have kinetic fragility of about 116 and 31, respectively, modeling fragile and moderately strong glasses (see Appendix A). Very strong glasses can also be modeled by introducing an additive offset to the particle hopping energy barrier [29], or by using a different form of  $g(V)$  and will be studied in the future. We subject the system to a cooling-heating cycle and study its out-of-equilibrium calorimetric responses. Using a direct construction method [28], we first prepare the system in thermodynamic equilibrium at some temperature  $T_0$  much higher than the glass transition temperature  $T_g$ . Then, we lower the bath temperature  $T$  at a constant rate  $\nu = |dT/dt|$ . Once  $T$  decreases to a temperature much lower than  $T_g$ , we reverse the process and heat up the system at the same rate  $\nu$  until  $T$  reaches  $T_0$ . See Appendix B for further information about the simulation details.

#### A. Energy and heat capacity

The energy per particle  $\varepsilon$  is monitored throughout the entire cooling-heating cycle. The specific heat  $c_v$  at constant volume is then calculated from  $c_v = d\varepsilon/dT$ .

Figures 1 and 2 display typical kinetic Monte Carlo simulation results for  $\varepsilon$  and  $c_v$  for cooling and heating rates  $\nu$  up to the slowest value  $\nu = 3 \times 10^{-4}$  that we can simulate. They successfully reproduce important features in experiments including energy and heat-capacity hysteresis with a prominent heat-capacity overshoot during heating [9,12,36]. Nevertheless, we also observe that  $c_v$  decreases more noticeably with  $T$  at large  $T$  than in experiments, which we attribute to a lack of particle vibrations and the large  $\nu$  used in the simulations (see Sec. IV A). The definition of the glass transition temperature  $T_g$  is given in Sec. III C.

Most importantly, Fig. 2 shows large values of  $c_v$  with a clear contrast between fragile and strong glasses. For  $\nu = 3 \times 10^{-4}$ ,  $c_v$  shoots up in the heating process to nearly  $12k_B$  for the fragile glass but only to about  $2.5k_B$  for the strong glass. These peak values of  $c_v$  occurring right above  $T_g$  characterize the magnitudes of the heat-capacity jumps. We have expressed  $c_v$  in unit of  $k_B$ , despite  $k_B = 1$ , to highlight that the dimensionless quantity  $c_v/k_B$  can be directly compared with experimental values. These values are of magnitudes similar to  $c_v$  jumps of, for example,  $8k_B$  and  $1.6k_B$  for toluene [37] and a typical metallic glass [4], which are fragile and moderately strong respectively. The DPLM has thus provided  $c_v$  jumps consistent with the experimental ones, which are significantly larger than those from conventional lattice models [24–26].

#### B. Fictive temperature and structural temperature

We identify the fictive temperature  $T_f$  of, in general, a nonequilibrium state with energy  $\varepsilon$  as a numerically

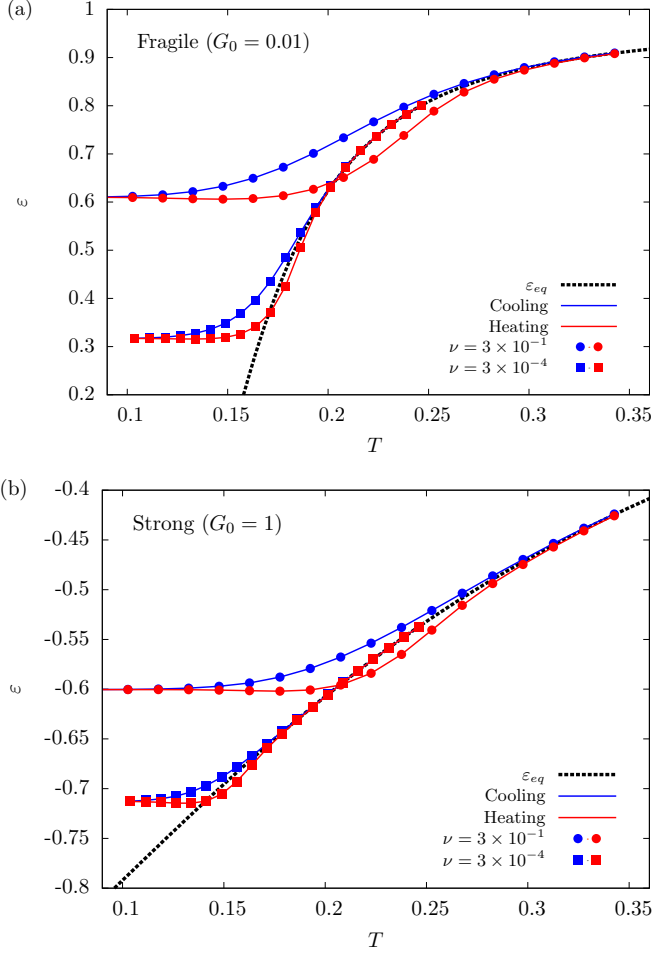


FIG. 1. Energy per particle  $\varepsilon$  during a cooling-heating cycle for (a) fragile glass with  $G_0 = 0.01$  and (b) strong glass with  $G_0 = 1$  at cooling and heating rate  $\nu$ . The black dashed lines show equilibrium energy  $\varepsilon_{eq}$  calculated from Eq. (8).

measurable structural temperature defined by [38]

$$\varepsilon = \varepsilon_{eq}(T_f), \quad (4)$$

where  $\varepsilon_{eq}$  is the equilibrium energy, which is calculated analytically by using Eq. (8) (see the discussion section below) and is given in Fig. 1 as black dashed line. Further details on  $\varepsilon_{eq}$  can be found in Appendix C. Thus,  $T_f$  measures the effective temperature of the particle interactions and reduces to the equilibrium temperature at equilibrium. Note that its dependence on the particle configuration is explicitly known and is thus, strictly speaking, not a “fictive” quantity. Figure 3 plots  $T_f$  against  $T$  for different  $\nu$  and  $G_0$  during a cooling-heating cycle by using the same simulation results leading to Fig. 1. We observe hysteresis in the evolution of  $T_f$  analogous to that of  $\varepsilon$  in Fig. 1. It also closely resembles hysteresis of  $T_f$  observed in experiments [13].

### C. Normalized heat capacity and $T_g$

Besides particle energy and fictive temperature, the hysteresis can further be demonstrated by a normalized heat

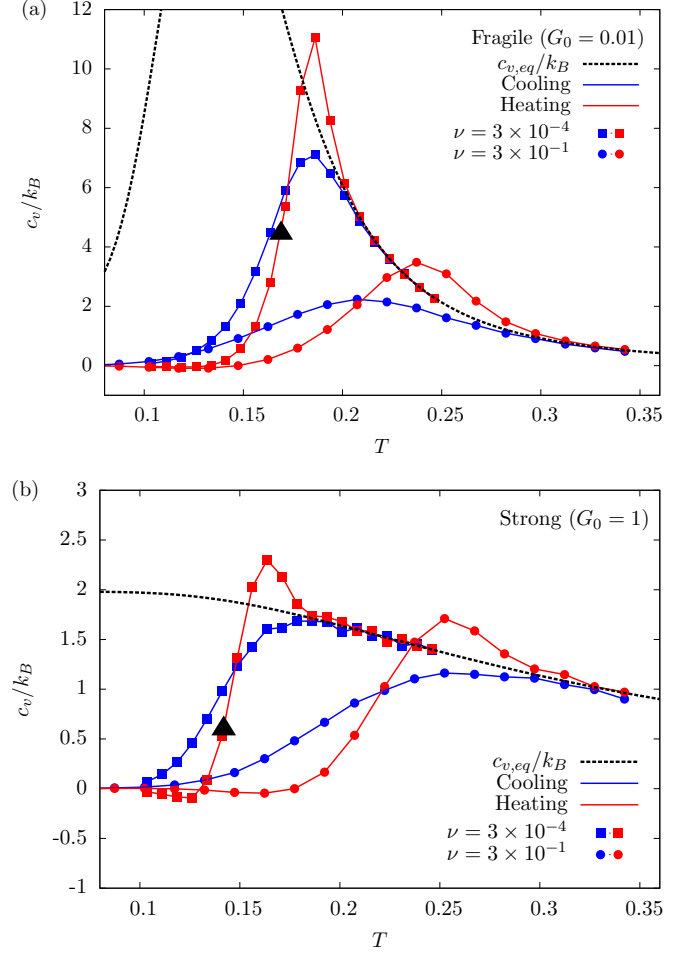


FIG. 2. Specific heat capacity  $c_v$  during a cooling-heating cycle for (a) fragile glass and (b) strong glass, with  $k_B = 1$ . The black dashed line shows the equilibrium specific-heat capacity  $c_{v,eq} = d\varepsilon_{eq}/dT$ , with  $\varepsilon_{eq}$  is calculated from Eq. (8). The black triangle marks the glass transition point measured from the heating data (see Sec. III C). Due to a lack of vibrations and the large  $\nu$  used,  $c_v$  and  $c_{v,eq}$ , which are more akin to heat-capacity excess, are close to 0 at small  $T$  and decrease rather significantly with  $T$  at large  $T$ .

capacity per particle defined as

$$\tilde{c}_v = \frac{c_v}{c_{v,eq}}, \quad (5)$$

where  $c_{v,eq} = d\varepsilon_{eq}/dT$  is the equilibrium specific-heat capacity. Using the fictive temperature  $T_f$  defined in Eq. (4), it can alternatively be expressed as

$$\tilde{c}_v = \frac{dT_f}{dT}, \quad (6)$$

a form more readily applicable to experiments [8,39]. The insets in Figs. 3(a) and 3(b) show  $\tilde{c}_v$  versus  $T$  for the fragile ( $G_0 = 0.01$ ) and strong ( $G_0 = 1$ ) glasses, respectively. The results again closely resemble those observed in experiments [8,39]. In particular,  $\tilde{c}_v$  approaches 0 for  $T \ll T_g$  both in our simulations and in experiments.

In contrast to  $c_v$ , the hysteresis loops exhibited by  $\tilde{c}_v$  for fragile and strong glasses closely resemble each other. This suggests that the more pronounced hysteresis of  $c_v$  for

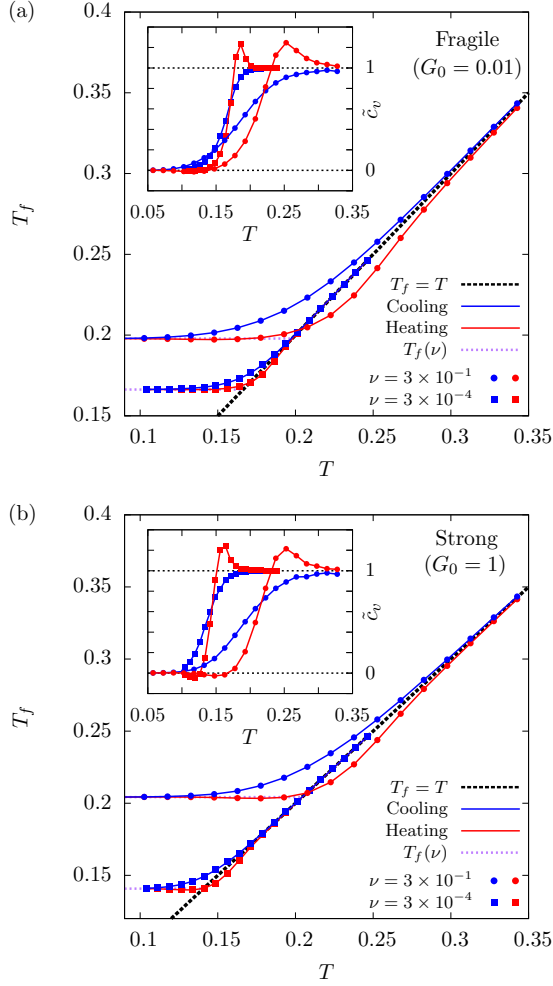


FIG. 3. Plot of fictive temperature  $T_f$  against bath temperature  $T$  at cooling and heating rates  $\nu$  for (a) fragile and (b) strong glasses. The black dashed line is the reference line  $T_f = T$ . The purple dotted lines indicate the fictive temperature  $T_f(\nu)$  in the glass limit. Insets in both (a) and (b): Normalized heat capacity per particle  $\tilde{c}_v$  versus bath temperature  $T$  obtained using Eq. (5).

fragile glass mainly originates from the large value of  $c_{v,\text{eq}}$  close to  $T_g$ .

We have adopted the glass transition temperature  $T_g$  based on  $\tilde{c}_v$  defined as the temperature at which  $\tilde{c}_v = 0.5$  as illustrated in Fig. 4. By drawing a tangent of  $\tilde{c}_v$  at  $T_g$ , the onset temperature  $T_{g,0}$  and the termination temperature  $T_{g,1}$  of the glass transition can also be defined.

#### D. Angell plot based on cooling rate $\nu$

Following Sec. III B, we measure at the end of cooling the fictive temperature  $T_f(\nu)$ , which is often considered close to  $T_g$  at small  $\nu$ . Here  $T_f(\nu)$  is the glass limit of the instantaneous fictive temperature  $T_f(T, \nu)$  after cooling to temperature  $T$  as given in Fig. 3, i.e.,  $T_f(\nu) = \lim_{T \rightarrow 0} T_f(T, \nu)$ . Based on this definition,  $1/\nu$  is a measure of the system relaxation time at temperature  $T_f(\nu)$ . The results are thus displayed in the style of an Angell plot in Fig. 5, where  $1/\nu$  is plotted against  $T_f(\nu_0)/T_f(\nu)$  with  $\nu_0 = 3 \times 10^{-4}$ . Results are similar to previ-

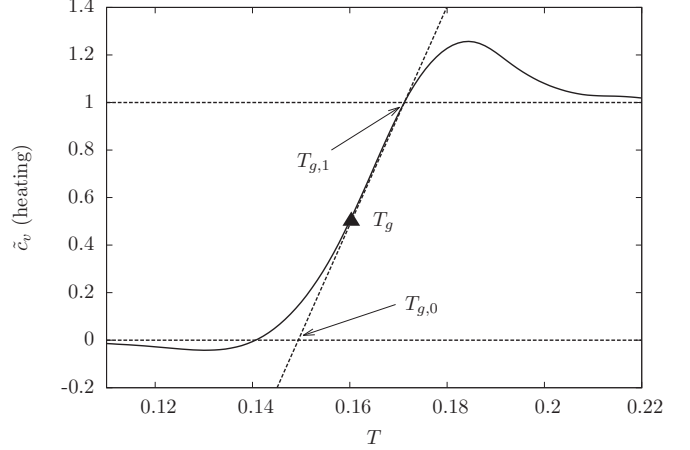


FIG. 4. Schematic diagram showing the definition of  $T_g$ ,  $T_{g,0}$ , and  $T_{g,1}$ .

ous studies with both Arrhenius [6] and super-Arrhenius [40] behaviors have been observed.

#### E. Heat-capacity overshooting magnitude

The  $c_v$  hysteresis as shown in Fig. 2 is more pronounced for the fragile than for the strong glass in agreement with experiments [9,12]. The correlation is further quantified in Fig. 6, where the maximum value of  $c_v$  during overshoot in the heating process, denoted by  $c_v^{\text{max}}$ , is plotted versus the kinetic fragility index  $m_k$  at various heating rates  $\nu$ . Note that  $m_k = \partial \log \tau / \partial (T_g^*/T)|_{T_g^*}$  is calculated using data from Fig. 10. We have used a reference relaxation time of  $\tau_r = 10$  to define the glass transition temperatures  $T_g^*$ , which is about the longest timescale we can simulate but is indeed small when compared to experiments (see Appendix A for further details). This leads to  $m_k$  much smaller than the experimental ones, as explained in detail in Ref. [29]. From Fig. 6,  $c_v^{\text{max}}$  is seen increasing with  $m_k$ . It is also observed that the heating

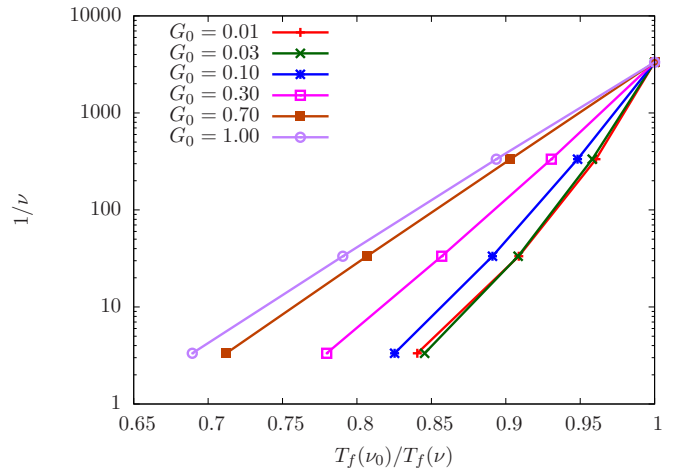


FIG. 5. Angell plot of reciprocal cooling and heating rate  $\nu^{-1}$  versus reciprocal fictive temperature  $T_f(\nu_0)^{-1}$  normalized by  $T_f(\nu)$  where  $\nu_0 = 3 \times 10^{-4}$ .



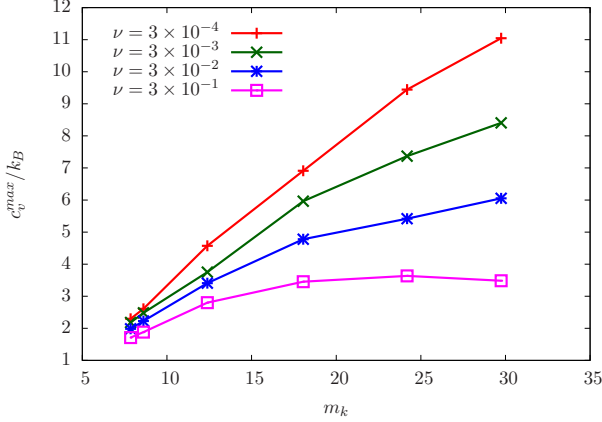


FIG. 6. Correlation between peak value  $c_v^{\max}$  of  $c_v$  during heating and kinetic fragility  $m_k$ .

rate affects  $c_v^{\max}$  for fragile glass more than for strong glass, a feature that has been observed in experiments [12].

#### F. Asymmetry in hysteresis loop

We now study the energy difference per particle  $\Delta\varepsilon$  at temperature  $T$  during cooling compared with heating following Ref. [39]. The insets of Fig. 7 plot  $\Delta\varepsilon$  against  $T/T_f(\nu)$  for strong ( $G_0 = 1$ ) and fragile ( $G_0 = 0.01$ ) glasses, at  $\nu = 3 \times 10^{-1}$  and  $3 \times 10^{-4}$ , where  $\Delta\varepsilon$  is obtained by subtracting  $\varepsilon$  from cooling by that from heating in Fig. 1. In each case, we observe a peak which is in general skewed. The skewness can be quantified by an asymmetric factor  $F_2/F_1$ , where  $F_1$  is the left half width at half maximum (HWHM) of the peak while  $F_2$  is the right HWHM. The main figure of Fig. 7 plots  $F_2/F_1$  against the kinetic fragility  $m_k$  for  $\nu = 3 \times 10^{-4}$ , which qualitatively resembles experimental results [39]. The asymmetry arises from the highly nonlinear temperature dependence of the relaxation dynamics, which can be analyzed using the Tool-Narayanaswamy-Moynihan-Hodge equations as shown

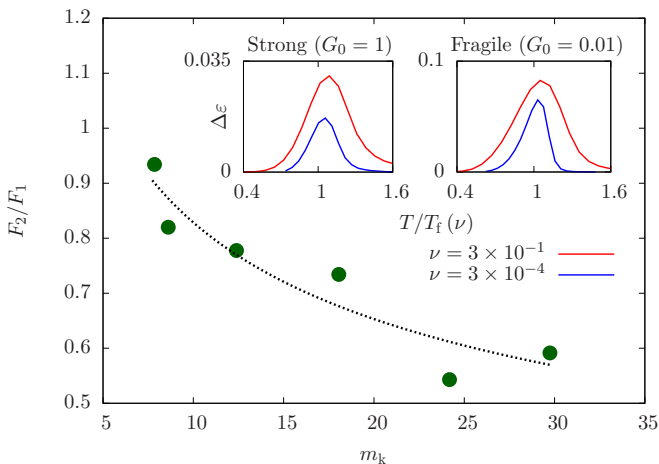


FIG. 7. Asymmetric factor  $F_2/F_1$  against kinetic fragility  $m_k$ , at cooling rate  $\nu = 3 \times 10^{-4}$ . Insets: Energy difference per particle  $\Delta\varepsilon$  against rescaled temperature  $T/T_f(\nu)$  for (left panel) strong glass ( $G_0 = 1$ ) and (right panel) fragile glass ( $G_0 = 0.01$ ).

in Ref. [39]. Our results show that the DPLM is able to naturally reproduce the trend of a stronger hysteresis asymmetry of the fragile glasses compared with strong glasses.

## IV. DISCUSSIONS

### A. Energy and heat-capacity hysteresis

Using the DPLM, we have reproduced the energy and heat-capacity hysteresis during cooling-heating cycles typical of glasses as shown in Figs. 1 and 2. While the main features of these hysteresis loops are captured, there are also some discrepancies, which we attribute to a lack of particle vibrations and the large  $\nu$  used in the simulations.

First,  $c_v$  from Fig. 2 is much closer to 0 at small  $T$  than in experiments. This is easily understandable as the DPLM does not simulate particle vibrations. A particle configuration corresponds to an inherent structure and  $\varepsilon$  represents the configurational energy [41]. In the glass phase at  $T \ll T_g$  with frozen configurations, the particle energy  $\varepsilon$  thus approaches a constant resulting at  $c_v \simeq 0$ . In fact,  $c_v$  in the DPLM can better be compared with heat-capacity excess from experiments, which is also close to zero in the glass phase [42].

Second, we observe that  $c_v$  decreases more noticeably with  $T$  at large  $T$  than in experiments. This results from a similar property of the equilibrium heat capacity  $c_{v,\text{eq}}$ . Due to the lack of vibrations in the DPLM, the particle energy  $\varepsilon$  attains a finite limit as  $T \rightarrow \infty$ , similar to the case of typical lattice models in statistical physics. This implies a diminishing  $c_v$  at large  $T$ , in contrast to typically molecular systems. An additional factor is that the adopted heating and cooling rates  $\nu$  are many orders larger than the experimental range. For example, for the fragile glass at  $\nu = 3 \times 10^{-4}$ , hysteresis occurs over  $T$  ranging from  $T \simeq 0.13$  to  $0.20$ , leading to a width  $0.07$  of the hysteresis as observable in Fig. 2(a). This width is about 43% of  $T_g = 0.163$  and this ratio decreases as  $\nu$  decreases. In contrast, the width of the hysteresis loops extends over only about 10% of  $T_g$  in experiments due to the much lower cooling and heating rates [12]. Because of the much wider temperature range covered in our simulations, we observe from Fig. 2(a) a noticeable continuous decrease of  $c_v$  with  $T$  beyond the hysteresis, while  $c_v$  appears to approach a constant in experiments. We thus expect these different features between simulations and experiments to diminish if a much slower  $\nu$  can be used, which, however, is impractical computationally.

The hysteresis phenomenon observed here is similar to those in typical systems with finite response times and can be modeled for example by the Tool-Narayanaswamy-Moynihan theory [7]. The process can be understood as follows. At the beginning of the cooling process when  $T$  is high, the system equilibrates fast with a short structural relaxation time  $\tau$ , and the energy per particle  $\varepsilon$  closely follows the equilibrium value  $\varepsilon_{\text{eq}}$ . As  $T$  decreases,  $\tau$  increases. Following Deborah's condition [7], when  $T$  becomes so low that  $|d\tau/dt| = 1$ , i.e.,  $|d\tau/dT| = \nu^{-1}$ , the system cannot fully equilibrate and falls out of equilibrium. For slower (faster) cooling, this takes place at lower (higher)  $T$ . In the nonequilibrium state, the system partially retains its preceding state, which is the higher-temperature near-equilibrium state, leading to  $\varepsilon > \varepsilon_{\text{eq}}$ . The discrepancy  $\varepsilon - \varepsilon_{\text{eq}}$  widens as  $T$  decreases. When  $T$

drops to such a low temperature that  $|d\tau/dt| \gg 1$ , structural relaxation can hardly happen and  $\varepsilon$  freezes.

In contrast, at the beginning of the heating process, the system has a longer  $\tau$  inherent from its nonequilibrium state at lower temperature, leading to  $\varepsilon$  less than the previous value at the same  $T$  during cooling. This originates the observed hysteresis, which closes only at a temperature high enough so that  $|d\tau/dt| \ll 1$ .

### B. Heat-capacity jump

As aforementioned, the correlation reproduced above between  $c_v$  jump and fragility is mainly caused by equilibrium properties of the glasses. Note that from Fig. 2,  $c_{v,\text{eq}} \simeq c_v > 0$  well above  $T_g$  and  $c_{v,\text{eq}} \simeq c_v \simeq 0$  well below  $T_g$ . The magnitude of  $c_{v,\text{eq}}$  close to  $T_g$  basically dictates the jump of  $c_v$ . The contrast of  $c_v$  between fragile and strong glasses therefore reduces to a similar contrast in  $c_{v,\text{eq}}$ . Equilibrium thermodynamics stipulates that

$$c_{v,\text{eq}} = T \frac{dS}{dT} \quad (7)$$

under constant volume conditions, where  $S$  denotes the entropy per particle. Before a quantitative analysis, it is immediately understandable from Eq. (7) why a fragile glass has a large  $c_{v,\text{eq}}$ , and thus a large  $c_v$  jump. Specifically, as  $T$  decreases toward  $T_g$ , the entropy  $S$  of fragile glasses have been shown to admit a dramatic drop, which is associated with increasingly constrained kinetic pathways characteristic of the glass transition [29]. This precisely implies a large  $dS/dT$  close to  $T_g$  and thus, using Eq. (7), also a large  $c_{v,\text{eq}}$  and  $c_v$ .

Furthermore, it is instructive to compare the magnitude of  $c_{v,\text{eq}}$  with naive predictions from equipartition of energy, which is exact for harmonic intermolecular potentials. In the DPLM, realized interaction  $V_{s_i s_j}$  between neighboring sites  $i$  and  $j$  in Eq. (1) is time dependent because  $s_i$  and  $s_j$  change as particles move around. Each  $V_{s_i s_j}$  is hence a degree of freedom of the system. If its distribution takes a simple unimodal form close to that in a harmonic oscillator, then equipartition of energy suggests an average interaction of  $\sim k_B T/2$  above  $V_0$ , leading to a heat capacity of  $k_B/2$  per interaction. Assuming a small void density  $\phi_v$ , we get  $c_{v,\text{eq}} \simeq z k_B/4 = k_B$ , where  $z = 4$  is the lattice coordination number. A  $c_{v,\text{eq}}$  much larger than  $k_B$  for a fragile glass therefore requires that the distribution of  $V_{s_i s_j}$  must deviate drastically from a unimodal form, as in a bicomponent distribution, and this will be further explained below. Note that this estimate is in general distinct from  $(d/2)k_B$  from the Dulong-Petit law, where  $d$  is the spatial dimension.

Equilibrium properties of the DPLM including  $c_{v,\text{eq}}$  will now be analytically calculated. As derived in Ref. [28] and extensively verified numerically [28,29,38], particles in the DPLM arrange themselves at equilibrium in such a way that the realized interaction energy  $V_{s_i s_j}$  follows exactly the *a posteriori* distribution  $p_{\text{eq}}(V) = \frac{1}{\mathcal{N}} g(V) \exp(-V/k_B T)$ , where  $\mathcal{N} = \int dV g(V) e^{-V/k_B T}$  is a normalization factor. The equilibrium energy per particle is thus

$$\varepsilon_{\text{eq}} = \frac{z}{2} \int dV V p_{\text{eq}}(V) \quad (8)$$

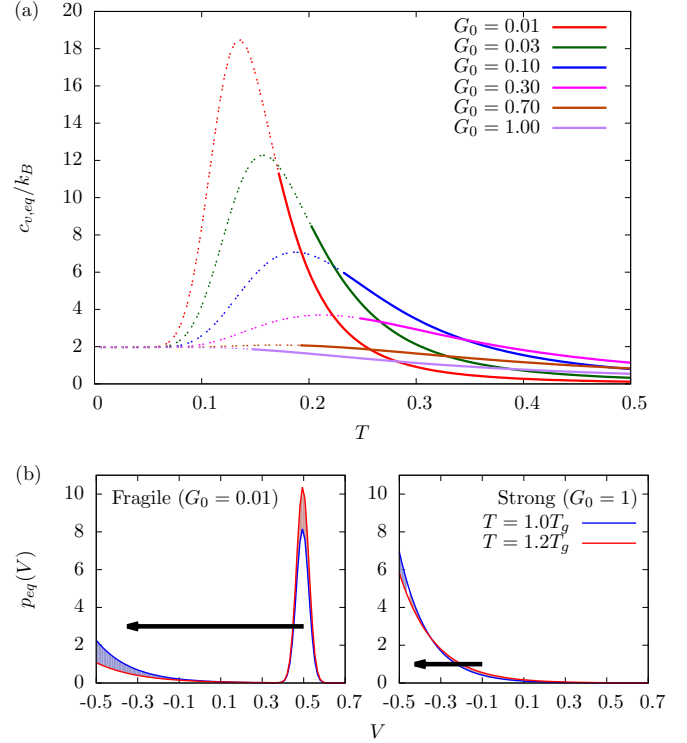


FIG. 8. (a). The temperature dependence of equilibrium specific-heat capacity  $c_{v,\text{eq}}(T)$  for various  $G_0$ . Physically unobservable data for  $T < T_g$  are plotted with dotted lines. (b). Equilibrium distribution  $p_{\text{eq}}(V)$  of interaction energy  $V$  at  $T_g$  (blue line) compared with that at  $1.2T_g$  (red line) for fragile glass (left panel) and strong glass (right panel). The loss in spectral weight of the high-energy interactions (red area) is balanced by the gain of the low-energy ones (blue area). Such weight transfer (black arrow) is much more substantial in fragile than in strong glass. For the ease of illustration, we have smoothed  $g(V)$  in Eq. (2) by replacing the uniform and the delta components by simple Fermi and Gaussian functions, respectively.

at small void density  $\phi_v$ . One then finds the equilibrium specific-heat capacity by  $c_{v,\text{eq}} = d\varepsilon_{\text{eq}}/dT$ , which is a more convenient expression than Eq. (7). With  $g(V)$  given by Eq. (2),  $\varepsilon_{\text{eq}}$  and  $c_{v,\text{eq}}$  can be explicitly worked out (see Appendix C), as already plotted in Figs. 1 and 2.

Figure 8(a) compares  $c_{v,\text{eq}}$  for various values of  $G_0$ . We observe that  $c_{v,\text{eq}}$  at  $T_g$  decreases monotonically with  $G_0$ . At the small  $T$  limit,  $c_{v,\text{eq}}$  converges to  $zk_B/2$  independent of  $G_0$ . This is because the low-energy uniform component of  $g(V)$  dominates, leading to effectively a unimodal situation with  $\varepsilon_{\text{eq}} \approx (z/2)(k_B T + V_0)$ . This leads to  $c_{v,\text{eq}} \simeq zk_B/2$  which differs from the equipartition prediction  $zk_B$  explained above only by a factor of 2. For the strong glass,  $zk_B/2$  directly approximates the  $c_v$  jump.

### C. Two-state picture

The increasingly prominent peak of  $c_{v,\text{eq}}$  in Fig. 8(a) as  $G_0$  decrease may seem to suggest an underlining criticality. However, there is no divergence at any finite  $G_0$ . Instead, the peak characterizes  $T$  at which the relative importance of the two components of  $g(V)$  in the two-state picture depends most sensitively on  $T$ . According to Eq. (8), the  $T$  dependence of

the particle energy  $\varepsilon_{\text{eq}}$  can be ultimately traced to a spectral weight transfer in the *a posteriori* distribution  $p_{\text{eq}}(V)$  from high-energy interactions to low-energy ones. This is illustrated in Fig. 8(b), where we compare  $p_{\text{eq}}(V)$  at  $1.2T_g$  with that at  $T_g$ . For the strong glass in Fig. 8(b) (right panel), a small probabilistic weight is transferred to interactions with energies lowered on average by about 0.35 (black arrow). In sharp contrast, for the fragile glass in Fig. 8(b) (left panel), the transfer is over an energy difference of about 0.9 (black arrow) and the weight of the low-energy part nearly doubles. Note that this contrast does not result from distinct energy scales, characterizable for example by  $k_B T_g$  which indeed take similar values of 0.149 and 0.163, respectively, for the strong and fragile glasses. The significant transfer for the fragile glass occurs due to a competition between entropy that favors the high-energy component of  $g(V)$  and the Boltzmann factor that favors its low-energy part, noting that the high-energy component has a much higher entropy due to its large weight of  $1 - G_0 = 0.99$  compared with the weight  $G_0 = 0.01$  of the low-energy part. Such a drastic spectral transfer is only possible due to the bicomponent form of  $g(V)$  highly relevant to fragile glasses, and is absent for the essentially unimodal form for strong glasses. Note that the transfer also causes the kinetic slowdown in fragile glasses [29] so that  $T_g$  occurs where  $c_{v,\text{eq}}$  varies sharply.

## V. CONCLUSION

To conclude, using the DPLM, we have reproduced the major experimentally observed features of the heat-capacity hysteresis of glass formers: the large value of  $c_v$  and the strong correlation with fragility. The large  $c_v$  jump of fragile glass during cooling below the glass transition temperature is demonstrated to be inherent from the large equilibrium value of  $c_v$ . Based on a two-state picture, the latter is shown to be controlled in turn by a crossover from a high-energy interaction state to a low-energy one, a process which also induces the high fragility. Our work shows that particle models defined on a lattice, in contrast to defect models, are capable of capturing glass thermodynamics intrinsically, with the essential physics intuitively revealed.

Note that using only the two-state model, one can already study simple kinetics by postulating superposition rules [43], but not complex dynamical phenomena. On the other hand, the DPLM can reproduce a wide range of characteristic glassy dynamics [28,29] and has also been successfully employed to address Kovacs paradox [38] and Kovacs effect [44] on glass aging. Our approach successfully combines the DPLM with the two-state picture, so that both thermodynamics and kinetics of strong and fragile glasses can be studied microscopically under a consistent set of assumptions. Investigating the rich phenomena exhibited by a diverse range of various glasses in such a unified manner should be of particular importance.

There have been interesting recent advancements in the study of the Kauzmann's paradox, which concerns the low temperature behaviors of the configurational entropy of glass [45,46]. The present DPLM nevertheless cannot be directly applied because the distinguishable nature of the particles leads to a divergence of the entropy in the large system size

limit, as detailed in the context of the Gibbs' paradox [47]. Note that particles in the DPLM are completely distinct from each other and cannot even be grouped approximately into a finite number of components, as have been suggested for polydisperse systems [45]. Alternatively, to study the Kauzmann's paradox, we have very recently generalized the DPLM to a model with  $M$  types of identical particles following random type-dependent particle interactions. Results will be reported elsewhere.

## ACKNOWLEDGMENTS

We thank helpful discussions with R. Shi and P. Sollich. This work was supported by General Research Fund of Hong Kong (Grant No. 15303220) and National Natural Science Foundation of China (Grant No. 11974297).

## APPENDIX A: GLASSY DYNAMICS

Following the procedures given in Ref. [29], we perform equilibrium simulations at various  $G_0$  and  $T$ . Then, we compute the self-intermediate scattering function defined as

$$F_s(\mathbf{k}, t) = \langle e^{i\mathbf{k} \cdot [\mathbf{r}_l(t) - \mathbf{r}_l(0)]} \rangle, \quad (\text{A1})$$

where  $\mathbf{r}_l$  is the position of particle  $l$  and  $k = 2\pi/\lambda$  with wavelength  $\lambda = 2$ . Figure 9 shows  $F_s(\mathbf{k}, t)$  versus time  $t$  for the fragile ( $G_0 = 0.01$ ) and strong ( $G_0 = 1$ ) glasses for various  $T$ . The structural relaxation time  $\tau$  is defined by  $F_s(\mathbf{k}, \tau) = e^{-1}$ . One can define a relaxation-time-based glass transition temperature  $T_g^*$  as the temperature at which  $\tau$  reaches  $\tau_r$ , where  $\tau_r = 10$  is a long relaxation time taken as a reference value. Figure 10 shows an Angell plot of  $\tau$  against  $T_g^*/T$ . As seen, the super-Arrhenius nature, and thus also the fragility, are enhanced monotonically as  $G_0$  decreases. We observe that  $G_0 = 0.01$  gives a fragile glass, while  $G_0 = 1$  gives a moderately strong glass. Glass with more Arrhenius behaviors can be simulated by adding a nonzero positive energy barrier offset to the particle hopping rate, as discussed in [29], or by modifying  $g(V)$  appropriately, which will be reported elsewhere.

Figure 11 shows a comparison between the heat-capacity-based  $T_g$  measured at  $\nu = 3 \times 10^{-4}$  and the relaxation-time-based  $T_g^*$  with  $\tau_r = 10$  for various  $G_0$ . As seen,  $T_g$  and  $T_g^*$  are quantitatively close to each other, as both  $\nu = 3 \times 10^{-4}$  and  $\tau_r = 10$  lead to similar modeled timescales, both of which lead to about the longest simulations we can perform. Increasing  $\nu$  or decreasing  $\tau_r$  can lead to increases in  $T_g$  and  $T_g^*$  respectively. On the other hand, the nonmonotonic dependence of  $T_g$  on  $G_0$  has been explained in Ref. [29]. The Angell plot based on relaxation time  $\tau$  in Fig. 10 gives a good indication of the kinetic fragility. Similar results are also obtained from a related Angell plot based on the diffusion coefficient  $D$ . Defining the glass transition as the point at which  $D$  decreases to a reference value  $D_r = 0.1$ , corresponding to the longest timescale we can simulate, the kinetic fragility  $m_k$  for  $G_0 = 0.01$  and 1 have been evaluated to be 26 and 7, respectively [29]. They should be compared with  $m_k = 4.7$  for an Arrhenius behavior under this definition. To see what materials these models correspond to, results have been extrapolated to a more realistic reference value of

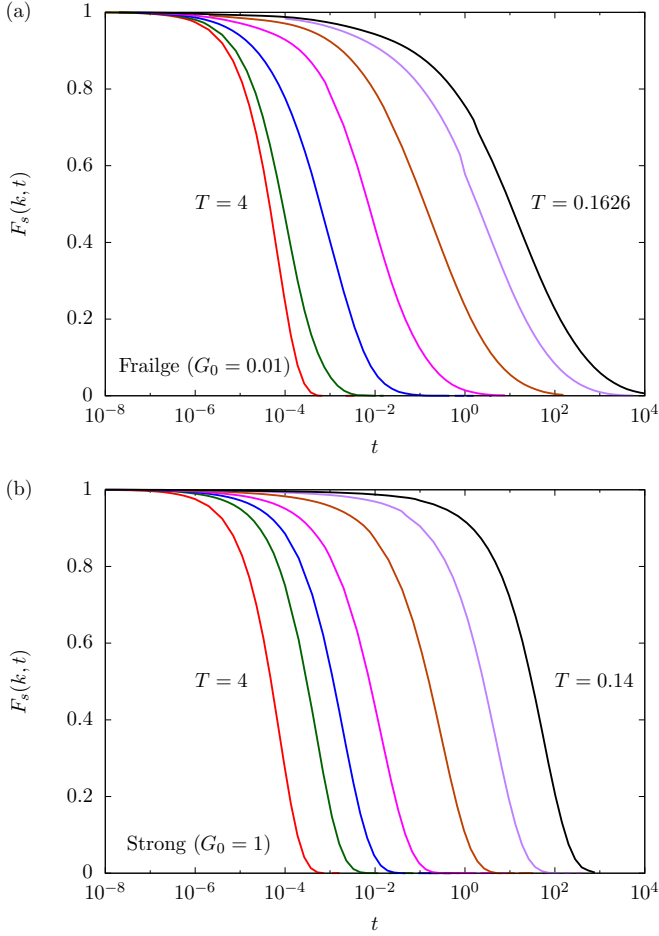


FIG. 9. Self-intermediate scattering function  $F_s(k, t)$  against time  $t$  for (a) fragile and (b) strong glasses with  $k = 2\pi/\lambda$  and  $\lambda = 2$ .

$D_r = 10^{-14}$ . This gives  $m_k \simeq 116$  for  $G_0 = 0.01$  [29], which is fragile and it is 4.5 times larger than the unextrapolated value of 26. The extrapolation scheme, however, cannot dis-

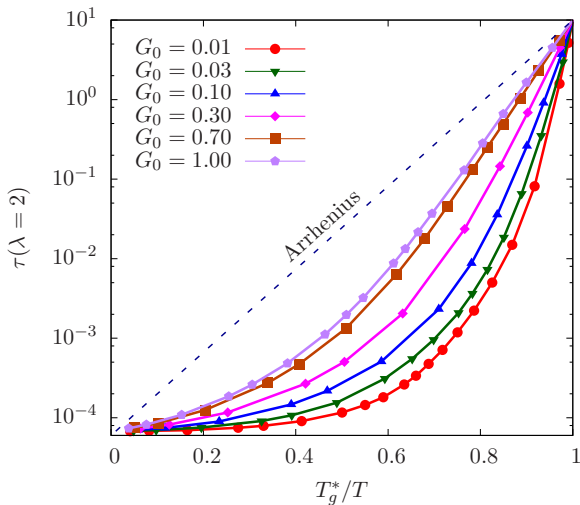


FIG. 10. Angell plot of relaxation time  $\tau$  for various  $G_0$ , with  $\lambda = 2$  and  $T_g^*$  defined at  $\tau = 10$ .

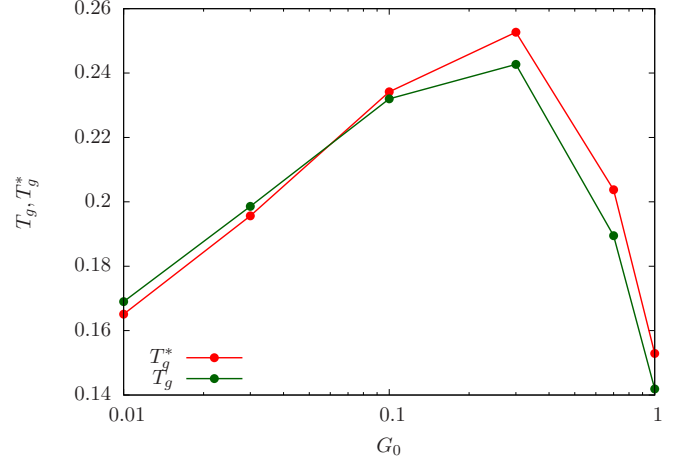


FIG. 11. Comparison between heat-capacity-based  $T_g$  measured at heating rate  $\nu = 3 \times 10^{-4}$  and relaxation-time-based  $T_g^*$  with reference time  $\tau_r = 10$  for various  $G_0$ .

criminate between the moderate strong glass at  $G_0 = 1$  from a strong glass. Instead, by analogy to the fragile glass, we simply estimate its fragility to be 4.5 times of the unextrapolated value, giving  $m_k \simeq 31$ . We thus suggest that the glasses with  $G_0 = 0.01$  and 1 model fragile and moderately strong glasses of fragilities around 116 and 31, respectively. Examples of them can be toluene and typical metallic glasses.

## APPENDIX B: SIMULATION DETAILS

Our simulation methods follow those explained in detail in Refs. [28,29]. For each run, we prepare an equilibrium sample at temperature  $T_0$  using an exact direct construction method by first equilibrating a simple lattice gas and then sample the realized interactions directly from the exact equilibrium particle interaction distribution. Particle dynamics are then simulated at any given temperature  $T$  using kinetic Monte Carlo method with Metropolis algorithm. We also apply accelerated algorithms including a rejection-free method. During simulations, we cool the system by lowering  $T$  in small steps of  $\Delta T$  after every time interval  $\Delta t$ , leading to a cooling rate of  $\nu = \Delta T/\Delta t$ . Cooling is performed until the temperature becomes much lower than  $T_g$ . Heating back up to  $T_0$  is then similarly performed.

We adopt a square lattice of linear size  $L = 200$ . Throughout the entire cooling-heating process, we measure the system energy according to Eq. (1). Each reported value is averaged over 50 measurements within a short period of time. For each set of values of  $G_0$  and  $\nu$ , data are further averaged over 100 independent runs. The longest run occurs at small  $G_0$  and takes up to about 120 h to complete on an Intel Xeon processor core.

## APPENDIX C: EQUILIBRIUM PROPERTIES

### 1. Equilibrium statistics

A surprising feature of the DPLM is that it has exactly solvable equilibrium statistics [28], predictions of which



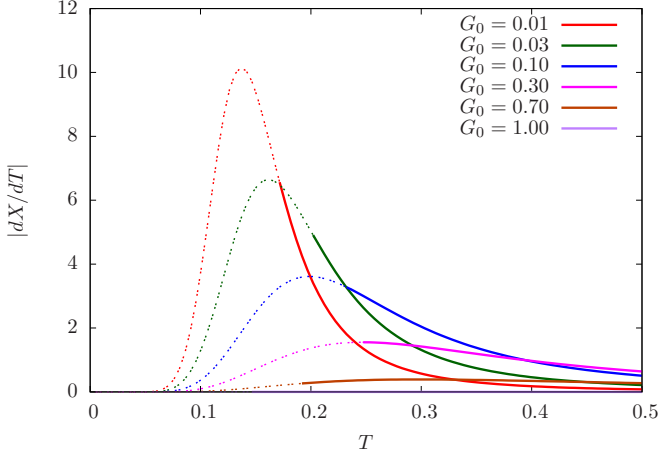


FIG. 12. Plot of  $|dX/dT| = -dX/dT$  against temperature  $T$  for various  $G_0$ , where  $X$  is the probabilistic weight of the low-energy component of the particle interaction distribution. Regions for  $T < T_g$  are plotted with dotted lines, where  $T_g$  is the glass transition defined in Fig. 4.

have been extensively and accurately verified numerically [28,29,38]. For the canonical ensemble considered in our DPLM simulations, the partition function  $Z$  in the thermodynamic limit is given by [28,29]

$$\frac{Z}{N!} = \sum_{\{n_i\}} e^{-\beta N_b U}, \quad (\text{C1})$$

where  $n_i = 0$  or  $1$  is the occupancy at site  $i$  and  $\beta = 1/k_B T$ . Also,  $N_b$  denotes the number of nearest-neighboring particle pairs and  $U$  is the free energy of a pair interaction defined by

$$U = -\frac{1}{\beta} \ln \mathcal{N}, \quad (\text{C2})$$

where

$$\mathcal{N} = \int dV g(V) e^{-\beta V}. \quad (\text{C3})$$

Interaction  $V_{s_i s_j}$  realized in the system at any instance follows the *a posteriori* distribution

$$p_{\text{eq}}(V) = \frac{1}{\mathcal{N}} g(V) \exp(-\beta V). \quad (\text{C4})$$

Based on the above equilibrium statistics, we now calculate the average energy and heat capacity. The equilibrium energy per particle  $\varepsilon_{\text{eq}}$  at small void density  $\phi_v$  can be calculated from Eq. (8), which can be rewritten as

$$\varepsilon_{\text{eq}} = \frac{z}{2} \frac{\partial \ln \mathcal{N}^{-1}}{\partial \beta}. \quad (\text{C5})$$

The equilibrium heat capacity  $c_{v,\text{eq}}$  is then obtained by taking the temperature derivative of Eq. (C5), which is given by

$$c_{v,\text{eq}} = \frac{z}{2} k_B \beta^2 \frac{\partial^2 \ln \mathcal{N}}{\partial \beta^2}. \quad (\text{C6})$$

Thus, the problem is reduced to calculating  $\mathcal{N}$ . For the bicomponent form of  $g(V)$  in Eq. (2), Eq. (C3) gives

$$\mathcal{N} = \frac{G_0}{\beta \Delta V} (e^{-\beta V_0} - e^{-\beta V_1}) + (1 - G_0) e^{-\beta V_1}. \quad (\text{C7})$$

Using Eqs. (C5)–(C7),  $\varepsilon_{\text{eq}}$  and  $c_{v,\text{eq}}$  can be evaluated numerically.

For various values of  $G_0$ ,  $c_{v,\text{eq}}$  is plotted in Fig. 8. We observe a strong dependence of  $c_{v,\text{eq}}$  on  $G_0$  and thus on the fragility. In particular, for the most fragile glass studied here with  $G_0 = 0.01$ ,  $c_{v,\text{eq}}$  shoots up to about  $18k_B$ , where  $k_B = 1$ . In sharp contrast, for the strong glass with  $G_0 = 1$ ,  $c_{v,\text{eq}} \leq 2k_B$ .

## 2. Bicomponent $g(V)$ and its two-state nature

For a better intuitive understanding of the large peak value of  $c_{v,\text{eq}}$  for fragile glass, we first derive further analytic expressions of  $c_{v,\text{eq}}$ . Following Ref. [29], the bicomponent interaction distribution  $g(V)$  in Eq. (2) can be rewritten as

$$g(V) = g_A(V) + g_B(V), \quad (\text{C8})$$

with the labels A and B specifying the two components, i.e.,

$$g_A(V) = \frac{G_0}{\Delta V}, \quad (\text{C9})$$

$$g_B(V) = (1 - G_0) \delta(V - V_1), \quad (\text{C10})$$

where  $V \in [V_0, V_1]$  with  $V_0 = -0.5$ ,  $V_1 = 0.5$ , and  $\Delta V = V_1 - V_0 = 1$ .

The probabilistic weight of the uniform component, i.e., component A, equals

$$X = \frac{\mathcal{N}_A}{\mathcal{N}_A + \mathcal{N}_B}, \quad (\text{C11})$$

while the weight for the Dirac distribution component is  $1 - X$ , with

$$\mathcal{N}_{A,B} = \int dV g_{A,B}(V) e^{-V/k_B T}. \quad (\text{C12})$$

Limiting to any one of the components, the equilibrium interaction distribution is

$$p_{\text{eq}}^{A,B} = \frac{1}{\mathcal{N}_{A,B}} g_{A,B}(V) e^{-V/k_B T}. \quad (\text{C13})$$

The average interaction energy within each component is simply computed by

$$\bar{V}_{A,B} = \int dV V p_{\text{eq}}^{A,B}(V). \quad (\text{C14})$$

Inserting Eqs. (C9) and (C10) into Eqs. (C12) and (C14), we have [29]

$$\mathcal{N}_A = \frac{G_0 k_B T}{\Delta V} (e^{-V_0/k_B T} - e^{-V_1/k_B T}), \quad (\text{C15})$$

$$\mathcal{N}_B = (1 - G_0) e^{-V_1/k_B T}, \quad (\text{C16})$$

$$\bar{V}_A = V_0 + k_B T - \frac{\Delta V}{e^{\Delta V/k_B T} - 1}, \quad (\text{C17})$$

$$\bar{V}_B = V_0 + \Delta V. \quad (\text{C18})$$

We now express the thermodynamic properties of the DPLM based on these properties of the individual components. Using Eqs. (C15)–(C18) and Eq. (C11), Eq. (8) can be recast into:

$$\varepsilon_{\text{eq}} = \frac{z}{2}[X\bar{V}_A + (1 - X)\bar{V}_B]. \quad (\text{C19})$$

By differentiating it with respect to  $T$ , we arrive at

$$c_{v,\text{eq}} = \frac{z}{2} \left[ -\frac{dX}{dT}(\bar{V}_B - \bar{V}_A) + X \frac{d\bar{V}_A}{dT} \right], \quad (\text{C20})$$

after noting that  $d\bar{V}_B/dT = 0$ .

For  $k_B T \ll \Delta V$ , a condition under which the peak value of  $c_{v,\text{eq}}$  occurs, Eq. (C17) reduces to  $\bar{V}_A \simeq V_0 + k_B T$  and Eq. (C20) becomes

$$c_{v,\text{eq}} \simeq \frac{z}{2} \left[ -\frac{dX}{dT}(\Delta V - k_B T) + X k_B \right]. \quad (\text{C21})$$

Since  $k_B = \Delta V = 1$  and  $z = 4$ , the large peak value of  $c_{v,\text{eq}} \simeq 18$  for  $G_0 = 0.01$  in Fig. 8 in fact results from a large magnitude of  $dX/dT$ . Specifically,  $|dX/dT|$  rises to 10 at  $T \simeq 0.136$  corresponding to the peak of  $c_{v,\text{eq}}$  as shown in Fig. 12. This quantitatively demonstrates our suggestion that a large  $c_{v,\text{eq}}$  for fragile glass is caused by a dramatic shift in the probabilistic weights of the two components in  $g(V)$ .

- 
- [1] G. Biroli and J. P. Garrahan, Perspective: The glass transition, *J. Chem. Phys.* **138**, 12A301 (2013).
- [2] F. H. Stillinger and P. G. Debenedetti, Glass transition thermodynamics and kinetics, *Annu. Rev. Condens. Matter Phys.* **4**, 263 (2013).
- [3] Wei Hua Wang, Dynamic relaxations and relaxation-property relationships in metallic glasses, *Prog. Mater. Sci.* **106**, 100561 (2019).
- [4] H. B. Ke, P. Wen, and W. H. Wang, The inquiry of liquids and glass transition by heat capacity, *AIP Adv.* **2**, 041404 (2012).
- [5] C. Austen Angell, Heat capacity and entropy functions in strong and fragile glass-formers, relative to those of disordering crystalline materials, in *Glassy, Amorphous and Nano-Crystalline Materials: Thermal Physics, Analysis, Structure and Properties*, edited by J. Šesták, J. J. Mareš, and P. Hubík (Springer Netherlands, Dordrecht, 2011), p. 21.
- [6] C. T. Moynihan, A. J. Eastale, J. Wilder, and J. Tucker, Dependence of the glass transition temperature on heating and cooling rate, *J. Phys. Chem.* **78**, 2673 (1974).
- [7] I. M. Hodge, Enthalpy relaxation and recovery in amorphous materials, *J. Non-Cryst. Solids* **169**, 211 (1994).
- [8] A. S. Keys, J. P. Garrahan, and D. Chandler, Calorimetric glass transition explained by hierarchical dynamic facilitation, *Proc. Natl. Acad. Sci. USA* **110**, 4482 (2013).
- [9] P. Li, Y. Zhang, Z. Chen, P. Gao, T. Wu, and L.-M. Wang, Relaxation dynamics in the strong chalcogenide glass-former of Ge<sub>22</sub>Se<sub>78</sub>, *Sci. Rep.* **7**, 40547 (2017).
- [10] Q. Zheng, Y. Zhang, M. Montazerian, O. Gulbiten, J. C. Mauro, E. D. Zanotto, and Y. Yue, Understanding glass through differential scanning calorimetry, *Chem. Rev.* **119**, 7848 (2019).
- [11] Z. Chen, Y. Zhao, and L.-M. Wang, Enthalpy and dielectric relaxations in supercooled methyl m-toluate, *J. Chem. Phys.* **130**, 204515 (2009).
- [12] T. V. Tropin, J. W. P. Schmelzer, G. Schulz, and C. Schick, The calorimetric glass transition in a wide range of cooling rates and frequencies, in *The Scaling of Relaxation Processes*, edited by F. Kremer and A. Loidl (Springer International Publishing, Cham, 2018), p. 307.
- [13] Y. Tanaka and N. Sakamoto, Analysis of tnm model calculation for enthalpy relaxation based on the fictive temperature model and the configurational entropy model, *J. Non-Cryst. Solids* **473**, 26 (2017).
- [14] K. Kremer and G. S. Grest, Dynamics of entangled linear polymer melts: A molecular-dynamics simulation, *J. Chem. Phys.* **92**, 5057 (1990).
- [15] W. Kob and H. C. Andersen, Testing mode-coupling theory for a supercooled binary lennard-jones mixture i: The van hove correlation function, *Phys. Rev. E* **51**, 4626 (1995).
- [16] A. Ninarello, L. Berthier, and D. Coslovich, Models and Algorithms for the Next Generation of Glass Transition Studies, *Phys. Rev. X* **7**, 021039 (2017).
- [17] P. L. Krapivsky, S. Redner, and E. Ben-Naim, *A Kinetic View of Statistical Physics* (Cambridge University Press, Cambridge, UK, 2010).
- [18] K. Binder and W. Kob, *Glassy Materials and Disordered Solids: An Introduction to Their Statistical Mechanics* (World Scientific, Singapore, 2011).
- [19] G. H. Fredrickson and H. C. Andersen, Kinetic Ising Model of the Glass Transition, *Phys. Rev. Lett.* **53**, 1244 (1984).
- [20] R. G. Palmer, D. L. Stein, E. Abrahams, and P. W. Anderson, Models of Hierarchically Constrained Dynamics for Glassy Relaxation, *Phys. Rev. Lett.* **53**, 958 (1984).
- [21] G. Biroli and M. Mézard, Lattice Glass Models, *Phys. Rev. Lett.* **88**, 025501 (2001).
- [22] F. Ritort and P. Sollich, Glassy dynamics of kinetically constrained models, *Adv. Phys.* **52**, 219 (2003).
- [23] J. P. Garrahan, P. Sollich, and C. Toninelli, Kinetically constrained models, in *Dynamical Heterogeneities in Glasses, Colloids and Granular Media*, edited by L. Berthier, G. Biroli, J.-P. Bouchaud, L. Cipelletti, and W. van Saarloosand (Oxford University Press, Oxford, UK, 2011).
- [24] G. H. Fredrickson and S. A. Brawer, Monte carlo investigation of a kinetic ising model of the glass transition, *J. Chem. Phys.* **84**, 3351 (1986).
- [25] G. D. McCullagh, D. Cellai, A. Lawlor, and K. A. Dawson, Finite-energy extension of a lattice glass model, *Phys. Rev. E* **71**, 030102(R) (2005).
- [26] Y. Nishikawa and K. Hukushima, Lattice Glass Model in Three Spatial Dimensions, *Phys. Rev. Lett.* **125**, 065501 (2020).
- [27] G. Biroli, J.-P. Bouchaud, and G. Tarjus, Are defect models consistent with the entropy and specific heat of glass formers? *J. Chem. Phys.* **123**, 044510 (2005).
- [28] L.-H. Zhang and C.-H. Lam, Emergent facilitation behavior in a distinguishable-particle lattice model of glass, *Phys. Rev. B* **95**, 184202 (2017).

- [29] C.-S. Lee, M. Lulli, L.-H. Zhang, H.-Y. Deng, and C.-H. Lam, Fragile Glasses Associated with a Dramatic Drop of Entropy Under Supercooling, *Phys. Rev. Lett.* **125**, 265703 (2020).
- [30] C. T. Moynihan and C. A. Angell, Bond lattice or excitation model analysis of the configurational entropy of molecular liquids, *J. Non-Cryst. Solids* **274**, 131 (2000).
- [31] D. Turnbull and M. H. Cohen, Free-volume model of the amorphous phase: Glass transition, *J. Chem. Phys.* **34**, 120 (1961).
- [32] A. Widmer-Cooper and P. Harrowell, Free volume cannot explain the spatial heterogeneity of debye-waller factors in a glass-forming binary alloy, *J. Non-Cryst. Solids* **352**, 5098 (2006).
- [33] X. Ma, Z. S. Davidson, T. Still, R. J. S. Ivancic, S. S. Schoenholz, A. J. Liu, and A. G. Yodh, Heterogeneous Activation, Local Structure, and Softness in Supercooled Colloidal Liquids, *Phys. Rev. Lett.* **122**, 028001 (2019).
- [34] V. Bapst, T. Keck, A. Grabska-Barwińska, C. Donner, E. D. Cubuk, S. S. Schoenholz, A. Obika, A. W. R. Nelson, T. Back, D. Hassabis, and P. Kohli, Unveiling the predictive power of static structure in glassy systems, *Nat. Phys.* **16**, 448 (2020).
- [35] C.-T. Yip, M. Isobe, C.-H. Chan, S. Ren, K.-P. Wong, Q. Huo, C.-S. Lee, Y.-H. Tsang, Y. Han, and C.-H. Lam, Direct Evidence of Void-Induced Structural Relaxations in Colloidal Glass Formers, *Phys. Rev. Lett.* **125**, 258001 (2020).
- [36] P. Badrinarayanan, W. Zheng, Q. Li, and S. L. Simon, The glass transition temperature versus the fictive temperature, *J. Non-Cryst. Solids* **353**, 2603 (2007).
- [37] C. Alvarez-Ney, J. Labarga, M. Moratalla, J. M. Castilla, and M. A. Ramos, Calorimetric measurements at low temperatures in toluene glass and crystal, *J. Low Temp. Phys.* **187**, 182 (2017).
- [38] M. Lulli, C.-S. Lee, H.-Y. Deng, C.-T. Yip, and C.-H. Lam, Spatial Heterogeneities in Structural Temperature Cause Kovacs' Expansion Gap Paradox in Aging of Glasses, *Phys. Rev. Lett.* **124**, 095501 (2020).
- [39] M. X. Li, P. Luo, Y. T. Sun, P. Wen, H. Y. Bai, Y. H. Liu, and W. H. Wang, Significantly enhanced memory effect in metallic glass by multistep training, *Phys. Rev. B* **96**, 174204 (2017).
- [40] Y. Yue, R. von der Ohe, and S. L. Jensen, Fictive temperature, cooling rate, and viscosity of glasses, *J. Chem. Phys.* **120**, 8053 (2004).
- [41] H.-Y. Deng, C.-S. Lee, M. Lulli, L.-H. Zhang, and C.-H. Lam, Configuration-tree theoretical calculation of the mean-squared displacement of particles in glass formers, *J. Stat. Mech.* (2019) 094014.
- [42] C. Austen Angell, Insights into phases of liquid water from study of its unusual glass-forming properties, *Science* **319**, 582 (2008).
- [43] R. Shi, J. Russo, and H. Tanaka, Origin of the emergent fragile-to-strong transition in supercooled water, *Proc. Natl. Acad. Sci. USA* **115**, 9444 (2018).
- [44] M. Lulli, L.-H. Zhang, C.-S. Lee, H.-Y. Deng, and C.-H. Lam, Kovacs effect in glass with material memory revealed in non-equilibrium particle interactions, [arXiv:1910.10374](https://arxiv.org/abs/1910.10374).
- [45] M. Ozawa and L. Berthier, Does the configurational entropy of polydisperse particles exist? *J. Chem. Phys.* **146**, 014502 (2017).
- [46] L. Berthier, M. Ozawa, and C. Scalliet, Configurational entropy of glass-forming liquids, *J. Chem. Phys.* **150**, 160902 (2019).
- [47] M. Toda, R. Kubo, and N. Saito, *Statistical Physics I: Equilibrium Statistical Mechanics* (Springer, Heidelberg, 1991).